Nanoscale

PAPER

View Article Online
View Journal | View Issue

Cite this: *Nanoscale*, 2016, **8**, 1627

Influence of growth temperature on bulk and surface defects in hybrid lead halide perovskite films†

Weina Peng,‡[a] Benoy Anand,‡[b] Lihong Liu,[a] Siddharth Sampat,[b] Brandon E. Bearden,[a] Anton V. Malko*[b] and Yves J. Chabal*[a]

Received 9th September 2015,
Accepted 12th December 2015

DOI: 10.1039/c5nr06222e

www.rsc.org/nanoscale

The rapid development of perovskite solar cells has focused its attention on defects in perovskites, which are gradually realized to strongly control the device performance. A fundamental understanding is therefore needed for further improvement in this field. Recent efforts have mainly focused on minimizing the surface defects and grain boundaries in thin films. Using time-resolved photoluminescence spectroscopy, we show that bulk defects in perovskite samples prepared using vapor assisted solution process (VASP) play a key role in addition to surface and grain boundary defects. The defect state density of samples prepared at 150 °C (~10^{17} cm^{-3}) increases by 5 fold at 175 °C even though the average grains size increases slightly, ruling out grain boundary defects as the main mechanism for the observed differences in PL properties upon annealing. Upon surface passivation using water molecules, the PL intensity and lifetime of samples prepared at 200 °C are only partially improved, remaining significantly lower than those prepared at 150 °C. Thus, the present study indicates that the majority of these defect states observed at elevated growth temperatures originates from bulk defects and underscores the importance to control the formation of bulk defects together with grain boundary and surface defects to further improve the optoelectronic properties of perovskites.

1. Introduction

Renewable energy generation and storage are indisputably the greatest challenges of the 21st century. The ever increasing need for low-cost ultrathin photovoltaic (PV) devices that can efficiently harness solar energy has motivated the search for alternate materials that can overcome the limitations of the conventional solar cell technology. In this regard, organic lead halide based perovskites have attracted considerable attention owing to their tunable band gap,[1] high absorption coefficient (>10^5 cm^{-1}) across the visible spectrum[2] and superior optoelectronic properties such as large diffusion length exceeding 1 micrometer,[3] high carrier mobilities, balanced ambipolar transport properties[4] and solution processability. Mesostructured or planar solar cells employing methylammonium lead trihalide perovskites ($CH_3NH_3PbI_3$ or $MAPbI_3$) and its substitutional variants have already reached efficiencies as high as 20.1%.[5] It has been shown that morphological properties can be controlled by varying the parameters of the preparation process including the annealing temperature,[6,7] the types of solvent and additives[8,9] and the specifics of the conversion process (vapor or liquid phase).[10,11] However, a comprehensive understanding of the intrinsic parameters that govern the optoelectronic properties of perovskite materials is still lacking, especially the role played by various type of defects. Recent correlated confocal photoluminescence (PL) and SEM imaging studies[12] demonstrated the existence of dark grains even in high-quality films, suggesting that further improvement in the performance of perovskite solar cells will likely require a more thorough understanding of the origin of defect states formed during the perovskite growth and their effects on the optoelectronic properties.

In general, defect states could be located on the perovskite surface, grain boundaries and within the bulk material. Effective surface passivation of perovskite has been demonstrated using iodopentafluorobenzene (IPFB)[13] and Lewis based salts,[14] which are believed to passivate uncoordinated halide and Pb ions respectively. In particular, the Lewis base treatment resulted in significantly longer PL lifetime and higher conversion efficiency highlighting the importance of defect passivation in perovskites. It has also been observed that increase in grain size and improvement in crystalline

[a]*Department of Material Science and Engineering, The University of Texas at Dallas, Richardson, TX 75080, USA. E-mail: chabal@utdallas.edu*
[b]*Department of Physics, The University of Texas at Dallas, Richardson, TX 75080, USA. E-mail: anton.malko@utdallas.edu*
†Electronic supplementary information (ESI) available. See DOI: 10.1039/c5nr06222e
‡These authors contributed equally to this work.

quality give rise to improved performance[15] for certain preparation procedures. The role of grain boundaries are debatable as certain theoretical predictions,[16] and electron beam induced current (EBIC) measurements[17] have shown that the grain boundaries of $CH_3NH_3PbI_3$ are electrically benign, as opposed to the common perception that grain boundaries act as recombination centers.[12] Interestingly, experimental results indicate that photon conversion efficiencies (PCEs) of unpassivated perovskite solar cells with very different grain sizes, *e.g.* microns *vs.* millimeters, can be similar[7,8,15,18] and in some cases are higher than those of surface passivated cells.[13,14] These facts suggest that there may be factors other than surface and grain boundary defects that contribute to lifetime decay and degrade the overall device performance.

In principle, low temperature solution processed perovskite materials are expected to be prone to bulk defect formation as well. However, the role of bulk defects is often ignored in perovskite devices since theoretical calculations suggest that the common bulk defects in perovskite, such as Pb vacancies and interstitial MA^+ ions which have the lowest formation energies, only form shallow acceptor or donor levels within the perovskite band gap.[19] Shockley–Read–Hall recombination theory[20] predicts that only deep level defect states act as efficient non-radiative recombination centers, resulting in impaired charge extraction efficiency. Therefore, low non-radiative recombination rates are expected for perovskite materials as evidenced by their high photoluminescence efficiency (nearly 70%) under high excitation power.[21] The recent PL microscopy studies concerning the photochemical passivation of traps in $CH_3NH_3PbI_3$ perovskites and its crystal size dependence provide preliminary experimental evidence for the existence of traps in the bulk of the material, in addition to surface defects.[22] Clearly more detailed investigations are needed in this direction in order to completely understand their behavior and effects.

In this work, we vary the synthesis temperature and use surface passivation methods to investigate the origin of defects in polycrystalline $MAPbI_3$ synthesized using the VASP technique. Using time-resolved photoluminescence spectroscopy and fluence dependent PL measurements, defects are characterized and their densities determined. Specifically, we show that bulk defects can be distinguished from surface defects that are passivated by water exposures, and are significant for samples processed at higher temperatures.

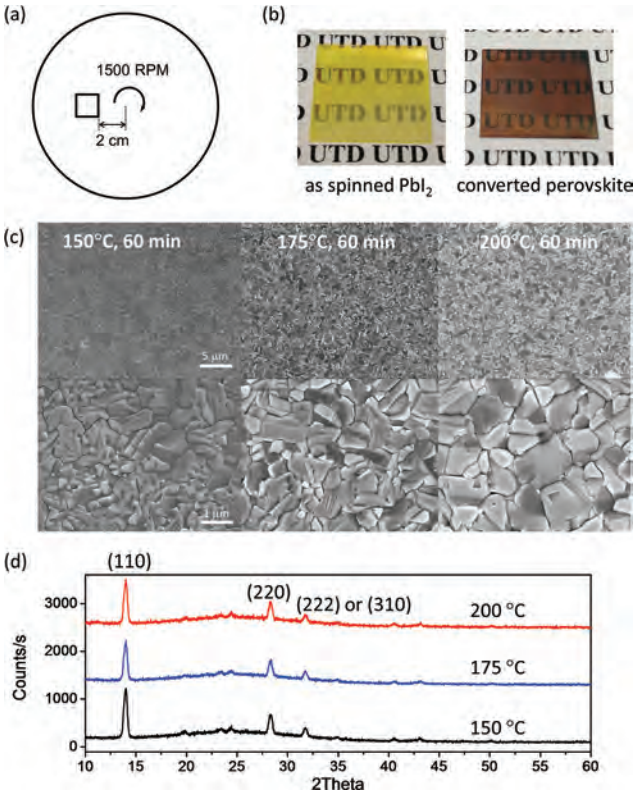

Fig. 1 (a) Schematic diagram of the 'off center' spin technique. (b) Photographic images of the as spun PbI_2 film (left) and the converted perovskite film (right). The metallic shiny color of the PbI_2 film indicates low surface roughness. (c) SEM images of the perovskite films prepared at three different temperatures: from left to right, 150 °C, 175 °C and 200 °C. Images at two different magnifications are shown for clarity. The scale bar of the upper images is 5 μm and that of the lower images is 1 μm. The images of each row share the same scale bar. (d) XRD spectra of the perovskite films prepared at three different temperatures. There is no evidence of the remaining PbI_2 phase, indicating complete conversion and no degradation of the film due to higher temperature annealing.

2. Experimental

2.1 Preparation of $CH_3NH_3PbI_3$ on glass

A thin layer (~160 nm) of $CH_3NH_3PbI_3$ is prepared according to the previously published VASP method.[10] Briefly, a uniform PbI_2 layer is first deposited on a piranha cleaned glass cover slide (18 mm × 18 mm) by spin casting PbI_2 dissolved in DMF solutions (200 mg ml^{-1}) at 1500 RPM for 60 s under atmospheric conditions. An off-center spinning position (Fig. 1a, described later) is used for the sample preparation. After the spinning, the film is heated at 150 °C for 20 minutes in an oven. Finally, it is converted into perovskites by exposing it to CH_3NH_3I vapor in a N_2 filled glove box. The conversion of PbI_2 to $CH_3NH_3PbI_3$ is performed at three different annealing temperatures (T_a) *viz.* 150 °C, 175 °C and 200 °C. The entire process takes approximately 60–90 minutes for completion, after which the initial metallic yellow colored PbI_2 film is transformed into a dark brown perovskite film, as shown in Fig. 1b. For XRD, PL and TRPL measurements, the sample is covered with a thin layer of PMMA to prevent the perovskite degradation due to interaction with the environmental moisture.

2.2 Time resolved PL measurements

PL measurements are performed using a microscope based PL system (μPL) employing confocal microscope (Olympus IX71), at room temperature. The perovskite film is excited with 400 nm laser pulses of ~120 fs pulse width from a pulse-

picked at 1.55 MHz, frequency doubled femtosecond Ti:sapphire oscillator (Coherent MIRA), using an Olympus air microscope objective (5×, 0.25 NA). The photoluminescence emission from the sample is passed through a spectrometer and recorded either with a CCD for spectral measurements or with a silicon avalanche photodiode (MicroPhoton Devices) for lifetime measurements. The PL decay histograms are collected *via* time-correlated single-photon counting (TCSPC) scheme performed on PicoHarp300 photon counting hardware (PicoQuant GmbH) with an overall time resolution of 50 ps.

2.3 Water treatment

The treatment is performed in a commercial ALD chamber (Savannah-100 system) at 50 °C under low vacuum and constant N_2 flow. The film is treated with different number of water pulses: 2, 4, 8 and 12 pulses. Each pulse lasts 30 ms and is followed by 50 s of N_2 purging. Immediately after the treatment, the film is covered with a protective PMMA layer in order to prevent further interaction between the film and the surrounding ambient environment.

3. Results and discussion

We find that the substrate position relative to the spin center plays a critical role in defining the morphology of the PbI_2 film, which in turn controls the final perovskite morphology due to template effects[10] of VASP. Spinning at the center results in fiber-shaped PbI_2 large crystals with smaller and denser branches evolving when a higher spin speed is used (see ESI† for details of morphology variation with the spin speed and substrate position). A smooth surface morphology across the entire substrate (RMS surface roughness $R_g \sim 6$ nm) can only be achieved when the substrate is placed 2 cm away from the spin center (see Fig. 1a). From the cross sectional SEM images (not shown here), the thickness of the PbI_2 layer is estimated to be ~110 nm, which yields a $CH_3NH_3PbI_3$ layer of 160 nm thickness after the VASP process. Moving the substrate further away from the center does not have any additional effect on the surface morphology except for the reduction in the final film thickness. The smooth PbI_2 film thus obtained is finally converted into a uniform perovskite film with low surface roughness ($R_g \sim 35$ nm). The increase in RMS roughness of the perovskite film comes from the rapid volume expansion during the incorporation of organic cations into the PbI_2 lattice. In addition, we observe that the PL lifetime is sensitive to the surface morphology of the sample (see ESI†). Therefore, in order to eliminate the discrepancies in PL lifetimes arising from the morphology variation among different samples, all the samples are prepared by keeping the parameters of our unique 'off center' spinning technique the same.

As shown in Fig. 1c, the average grain size of the 150 °C-grown perovskite film is approximately one micron. The morphology evolves gradually with the increase in synthesis temperature: the sample prepared at 200 °C shows the cleanest surface morphology with the least amount of facets and slightly larger grains. We also observe pinholes, with sizes on the order of 5 μm, present in the 200 °C film (see ESI†). These holes are clearly visible under the microscope and are intentionally avoided during the micro-PL (μPL) measurements (excitation and collection spots are <3 μm and are positioned tens of microns away from holes). Since the carrier diffusion length is approximately a micron, these holes will not have effects on the μPL measurements. The XRD spectra in Fig. 1d clearly show that no PbI_2 phase is present, suggesting complete perovskite conversion and absence of any degradation for all three processing temperatures. Preferential growth along the (110) direction is also observed, with (110) at 14.0° and (220) at 28.3° being the most prominent diffraction peaks. Previously it was reported that $MAPbI_3$ decomposes at elevated temperature (>100 °C in inert atmosphere).[23] However, with the continuous supply of MAI vapor during the VASP process, the sample is able to maintain a pure perovskite phase even when annealed at 200 °C for 60 min.

The optoelectronic properties of the as-prepared perovskite film are summarized in Fig. 2 for three different growth temperatures. Both PL intensity (Fig. 2a) and time resolved PL (TRPL) decay measurements (Fig. 2b) show similar trends for the growth temperature (T_a = 150 °C > 175 °C > 200 °C). The PL emission peak of the 150 °C sample is centered at 768 ± 1.5 nm (1.61 eV) with a full width at half maximum of ~40 nm, and slightly red shifted (by 2 nm) when T_a is increased. The shift observed in PL peak position is due to its strong correlation with the average grain size,[24] and is in agreement with the size variation seen in Fig. 1c. The PL intensity and lifetime are direct measures of the optical quality of a material as they correspond to the radiative recombination of the photogenerated carriers. When defects or trapping sites are present in the material, the photogenerated carriers get trapped at these sites and recombine non-radiatively, *i.e.* without emitting photons. Consequently, the photoluminescence efficiency is quenched and the lifetime is shortened. Thus from the PL characteristics summarized in Fig. 2a and b, it is apparent that there is a degradation of the film quality and introduction of more non-radiative defect centers as T_a is increased.

Upon an increase in excitation fluence, we observe the fastening of PL decays which progressively deviates from monoexponential behavior (can be approximated with bi-exponentials and later tri-exponentials fits, see ESI†). Such systematic behavior indicates the onset of additional recombination processes, with considerably different decay rates, as a function of the injected carrier density in agreement with earlier studies.[25] At low fluences (photogenerated carrier density $n_c < 10^{17}$ cm^{-3}), recombination of photogenerated carriers occurs mainly *via* slow monomolecular processes such as trap-assisted recombination, resulting in monoexponential PL decay as shown in Fig. 2b. At medium fluences (10^{17} $cm^{-3} < n_c < 10^{18}$ cm^{-3}), band-edge PL increases due to dominant bimolecular processes such as non-geminate/free carrier recombination. With further increase in excitation fluence ($n_c > 10^{18}$ cm^{-3}) fast, non-radiative, multiparticle processes such as

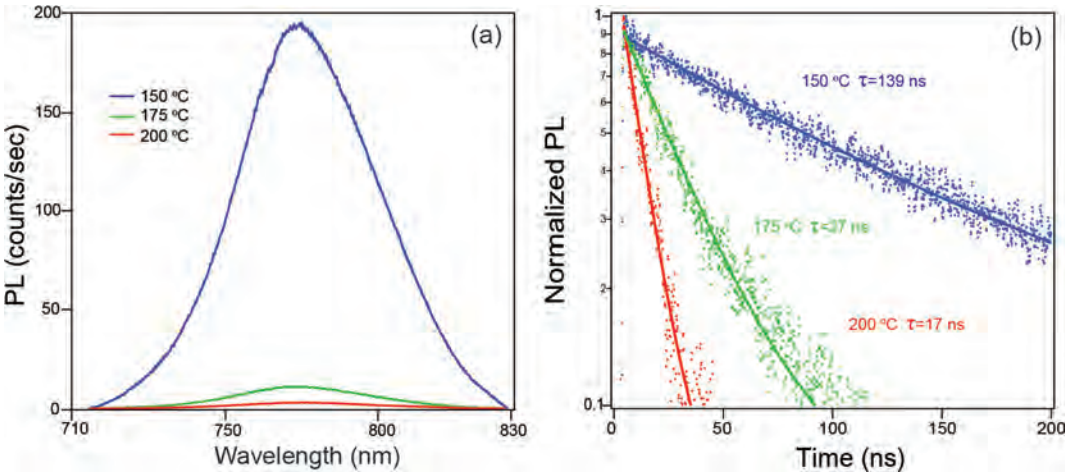

Fig. 2 Room temperature (a) PL spectra and (b) time resolved photoluminescence decay traces of the perovskite films prepared at three different temperatures under an excitation fluence of 0.36 μJ cm^{-2}. The experimental TRPL data is fitted with mono-exponential functions (solid lines).

Auger recombination are activated due to increased carrier–carrier interactions.[26] Such complex PL decay in perovskites are usually analyzed using rate equation based generic models which also provide additional information such as trap densities.[27,28] However for ease of representation we have followed a simple multi-exponential analysis in order to compare the different recombination processes in our samples. Interestingly the trend in lifetime values observed for low excitation fluence shown in Fig. 2b remains the same at all excitation densities and for all lifetime components establishing the fundamental temperature induced difference among the samples.

Following ref. 26, we estimated the trap density in perovskites from fluence dependent PL measurements. At low excitation fluence where non-radiative Auger losses are minimal, under the assumption that trap assisted recombination is considerably slower than band edge bimolecular recombination, the initial photogenerated charge carrier density $n_c(0)$ is given by:

$$n_c(0) = \sum_i n_{TP}^i(0)(1 - e^{-a_i \tau_0 I_{PL}/k}) + I_{PL}/k \qquad (1)$$

where I_{PL} is the integrated PL intensity which relates to the carrier density by $I_{PL} = k\int_0^\infty n_c(t)/\tau_0 dt$, where k is constant for a given sample, τ_0 is the PL lifetime, $n_{TP}^i(0)$ is the initial unfilled trap state density, and a_i is the product of the trap cross section and the carrier velocity (a parameter unique for each type of trap). The summation over i takes into account different types of traps: *e.g.*, in ref. 26 the perovskite film contains significant amount of both surface and bulk traps. According to eqn (1), the trap density can thus be determined by fitting the n_c *vs.* I_{PL} curve. Fig. 3 displays the photogenerated carrier density *vs.* the integrated PL intensity for our perovskite films grown at three temperatures. The solid lines represent the best fits obtained with eqn (1) and the fitting parameters are listed in Table 1.

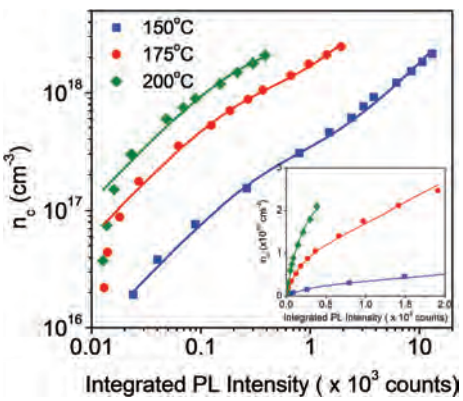

Fig. 3 Photo-excited carrier density n_c *vs.* the integrated PL density I_{PL} for perovskite films prepared at three different temperatures. Solid lines are numerical fits using eqn (1). Inset shows the regime of low integrated PL counts in linear scale.

Table 1 Fitting parameters for the n_c *vs.* I_{PL} curves of perovskite samples grown at three temperatures. The trap state density (n_{TP}) increases by an order of magnitude when the growth temperature is increased from 150 °C to 200 °C, resulting in considerable degradation of the PL characteristics

Annealing temperature (°C)	n_{TP} (cm^{-3})	$a \times \tau_0$ ($\times 10^{-3}$)
150	$(1.6 \pm 0.5) \times 10^{17}$	4.1 ± 2.0
175	$(0.8 \pm 0.3) \times 10^{18}$	9.1 ± 5.1
200	$(1.6 \pm 0.6) \times 10^{18}$	6.2 ± 1.8

Only one type of defects is sufficient to fit the data for all three annealing temperatures shown in Fig. 3. Adding another type of defects does not improve the poor fit observed in the region of low excited carrier concentrations. This region has a relatively large error bar due to the extremely low PL counts.

The deviation between the fits and the experimental data appears substantial in this region due to the log–log scale employed in Fig. 3, but looks completely negligible in a linear-linear scale as shown in ref. 26 and in the inset of Fig. 3. It is possible that the cross section of the surface and bulk defects are similar in our samples, thus making the accurate determination of their respective densities from a single fit difficult. Further, the phenomenological model presented above is not conclusive enough to address all the processes involved in this system since only one lifetime (τ_0) is considered in the model although the samples show higher order decays at elevated excitation densities. The n_{TP} value of the 150 °C-grown sample (1.6×10^{17} cm^{-3}) is close to the trap density estimated for polycrystalline perovskite films previously.[26] It is clear from Table 1 that the trap state density increases dramatically with increase in T_a, which corroborates the reduction in PL intensity and lifetime seen earlier (Fig. 2).

The n_c *vs.* I_{PL} plots shown in Fig. 3 are a representation of the PL efficiency of the samples and are indicative of their internal quantum efficiency (IQE). Considering the PV applications of perovskite, Yablonovitch and co-workers[29] have pointed out that high external fluorescence efficiency is a necessity for achieving high PV efficiency since additional non-radiative recombination channels impede the carrier buildup, limiting the achievable open-circuit voltage. In this regard, the present model captures the most important difference between the samples annealed at different temperatures despite its numerical simplicity, by only taking into account the varying trap density.

Table 1 shows that the trap density increases by almost 5 fold when T_a is raised by only 25 °C (*i.e.*, from 150 °C to 175 °C). Increasing the temperature to 200 °C causes a further reduction in IQE, even though the increase in trap density is merely a factor of 2. This indicates that most of the degradation happens between the temperature range of 150 °C and 175 °C. Previous theoretical calculations have predicted that the processing window for perovskite materials is rather narrow.[19] Our experimental results verify that the temperature window for the perovskite formation is indeed less than 25 °C for the VASP process. Below 150 °C, it takes a very long time to convert the sample while the sample quality heavily deteriorates when the growth temperature is increased above 175 °C.

Most of the previous work concerning the effects of annealing temperature in perovskite materials has focused on the changes in surface morphology. It is known that high temperature annealing affects the continuity of the film and induces holes,[6] similarly to the case of our 200 °C sample (Fig. 1(c)). Consequently, the electron transport layer (ETL) and hole transport layer (HTL) can form a direct contact through these holes, shunting the conducting path and lowering the solar cell performance. However the effect of T_a on defect density has not been addressed in detail yet. Our experimental results suggest that elevating T_a not only affects the uniformity of the film but also lowers its intrinsic quality by introducing more traps. Both factors impair PCE and hence have to be examined.

From the SEM characterizations presented in Fig. 1c we have seen that the average grain size of the samples increases gradually with T_a. If the majority of the trap states come from grain boundaries of the polycrystalline sample, increase in grain size must result in a reduction in trap density. However, our experimental results show exactly the opposite trend – the n_{TP} value rises remarkably when T_a increases indicating that the high temperature annealed sample (175 °C and 200 °C) must contain considerable amount of surface and/or bulk traps. In order to further distinguish between these two kinds of traps, we performed surface passivation of 200 °C-grown perovskite films with water vapor whose passivating role has been suggested by earlier studies.[13,18,30]

For perovskite materials, the role of water is two-fold. It is known that perovskite decomposes[31] ($CH_3NH_3PbI_3 \rightarrow PbI_2 + CH_3NH_2 + HI$) when the film is exposed to air for long time or under very humid conditions (*e.g.* when water condensation occurs). However, under moderate humidity conditions water facilitates the intercalation process, resulting in perovskite materials of better quality.[18] Furthermore, the potential passivating role of water on perovskites has been explicitly pointed out in ref. 13. The surface under-coordinated Pb ions are likely to form lead hydroxide when interacting with H_2O molecules. Therefore, controlled exposure to water vapor is expected to decrease the number of free Pb^{2+} ions on the perovskite surface.

The water vapor treatment was performed in a commercial ALD chamber at 50 °C under constant N_2 purging. The sample was treated with different number of pulses to make sure that surface saturation was achieved. It was found that for 2, 4 and 8 water pulses, there is no PbI_2 phase formed during the treatment, as indicated by the XRD spectra (Fig. 4a). When more than 8 H_2O pulses are used, the appearance of a tiny peak at 12.6° in the XRD spectrum indicates the formation of a small amount of PbI_2 (see ESI†). Finally, *in situ* FTIR studies (see ESI†) suggest that H_2O molecules interact solely with the perovskite surface without penetrating into the lattice under the treatment condition as the main FTIR modes from the organic cations are not affected after water exposure. Therefore, we confirm that the main effect of moderate water exposure is to passivate the surface alone.

The water treatment is found to considerably affect the PL properties of the 200 °C-grown perovskite films. As shown in Fig. 4b and c, the PL intensity of the 200 °C-grown sample increases by five times whereas the PL lifetime more than doubles after several water pulses. Similar PL results are obtained for the samples treated with 2, 4 and 8 H_2O pulses, indicating that saturated surface coverage has already been achieved with just 2 water pulses. Interestingly, increase to 12 H_2O pulses further increases the lifetime, which concurs with the introduction of PbI_2 phase in the sample (see ESI†). Previously, it was found that intentionally induced PbI_2 passivates the surface and grain boundaries of perovskite, thereby improving its optoelectronic properties.[32] Further discussion on the effect of PbI_2 is beyond the scope of the present study since it involves another passivation mechanism,

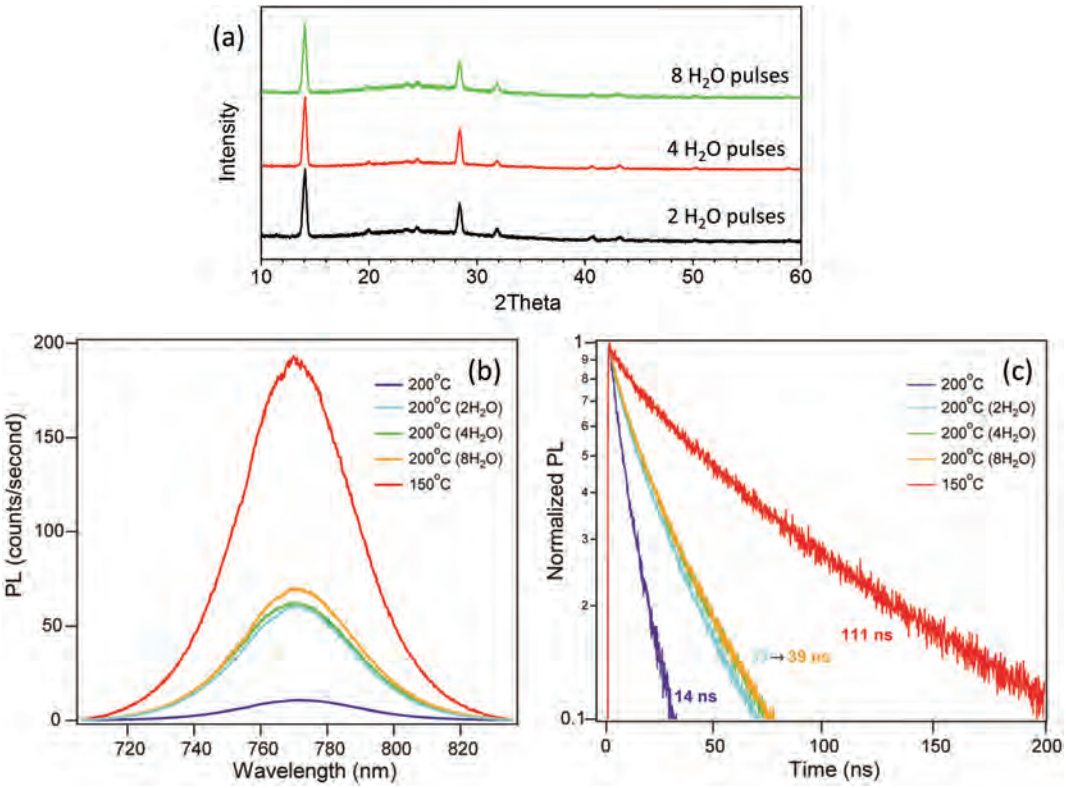

Fig. 4 (a) XRD spectra of the 200 °C-grown perovskite sample treated with 2, 4 and 8H_2O pulses. No structural degradation, which is indicated by the PbI_2 peak at 12.6°, can be observed. (b) PL spectra and (c) TRPL decay curves of 200 °C annealed samples treated with different number of water pulses. The PL intensity and decay traces of the untreated 150 °C and 200 °C grown samples are also shown as references. The excitation fluence is 0.36 μJ cm^{-2}, well within the monomolecular excitation regime.

different from the surface passivation caused by H_2O molecules. Both PL intensity and TRPL decay results support our assumption that water treatment passivates the perovskite surface, *i.e.* decreases the number of non-radiative recombination centers that can be attributed to surface trap sites. It is noteworthy that the lifetime of the water treated 200 °C-grown sample is still significantly lower (3–4 times) than that of an un-passivated 150 °C-grown sample, suggesting that surface passivation using H_2O cannot eliminate all the trap states present in the 200 °C-grown sample. But it has to be pointed out that the exact passivation mechanism of water molecules, *i.e.*, the type of atomic species on the perovskite surface which are targeted, will give additional perspectives to our discussion and is currently under investigation. Considering the relatively unknown nature of the perovskite surface (according to the author's best knowledge, there is no existing literature detailing the atomic structure of perovskite surface), a complete passivation of the perovskite surface with water molecules cannot be claimed here. It is possible that several chemical treatments are necessary to fully passivate the perovskite surface, but this is clearly out of the scope of this current paper. As discussed earlier, the difference observed in the optoelectronic properties between 150 °C and 200 °C grown samples is clearly not due to grain boundaries because the 200 °C-grown samples have larger grain size (fewer grain boundaries). Therefore to a first order approximation – most of the surface defects are passivated with water molecules – we deduce that a large proportion of the trap states in the high temperature annealed samples is likely to originate from the bulk, *i.e.* from states such as bulk vacancies that cannot be modified by water adsorption alone. Recently, similar conclusions on the existence of bulk traps have been drawn from PL studies carried out on perovskites containing dissolved O_2 wherein slow PL enhancement observed with thicker crystals are attributed to slow photochemical passivation of bulk traps (see ESI†).[22]

Even though the temperature range employed in the VASP method is higher (150–200 °C) than other solution processes (typically ~100 °C), it has the advantage to produce a more uniform surface morphology with full surface coverage thanks to its associated template effects, which is difficult to achieve with other solution spinning methods. The conversion is implemented by a continuous supply of CH_3NH_3I to ensure that PbI_2 is fully converted into perovskite with minimal thermal decomposition, which in turn results in high efficiency solar cells.[10] Theoretical calculations have predicted that deep level bulk defects in perovskites have higher for-

mation energies[19] in contrast to the more common shallow trap levels. Thus the VASP technique offers a unique temperature range to explore the optoelectronic properties of perovskites which is hard to achieve with other techniques such as one-step solution processing or sequential coating of PbI_2 and MAI, in which structural decomposition takes place well before the prevalent formation of bulk defects. In contrast, the relatively high temperature window offered by the VASP technique used here directly points to the important role of bulk defects in determining the optical properties of perovskites. Although the bulk defect density is much suppressed in the 150 °C-grown sample, the formation of the bulk defects is increased at higher annealing temperatures (~200 °C), as demonstrated by the increase in n_{TP}. Therefore, contrary to common belief, bulk defects cannot be completely neglected in perovskite materials as they have been shown to have a detrimental effect on their optoelectronic properties. For certain processing conditions, such as the high temperature annealed samples here, bulk defects will become the dominant factor in determining the perovskite properties. Considering the sensitivity of defect level towards T_a demonstrated in this work, a more precise control of the synthesis conditions is important to mitigate the adverse effects of bulk defects, which limit the PV performance of perovskite solar cells.

4. Conclusions

In summary, the VASP technique is used to synthesize polycrystalline perovskite films over a range of annealing temperatures (between 150 and 200 °C). The measurements reveal that, despite the slight increase in grain sizes found for samples produced at higher annealing temperature, their PL intensities and decay lifetimes strongly decrease as T_a is increased. Using fluence dependent PL measurements, we estimate the trap density in 150 °C-grown samples to be $\sim 10^{17}$ cm^{-3} and find that it increases by almost an order of magnitude for 200 °C-grown samples. The larger grain size of 200 °C grown samples rules out the possibility that grain boundaries are the main sources of defects in these samples. Although controlled water exposures are shown to passivate surfaces, the PL intensity of the well surface-passivated 200 °C-grown samples is only partially restored to approx. 30% of the values found for the 150 °C-grown samples, pointing towards the possible dominance of bulk trap states within the high temperature annealed perovskite films. Thus the present study highlights the existence of bulk defects and their decisive role in determining the optoelectronic properties of trihalide perovskites – an issue that was not sufficiently addressed in the past. More attention needs to be devoted to studies of the origins of bulk defects in perovskites in order to continue the optimization of solar conversion efficiencies.

This work was supported by the U.S. Department of Energy, Office of Science, Basic Energy Sciences, under Award # DE-SC0010697.

References

1 G. E. Eperon, S. D. Stranks, C. Menelaou, M. B. Johnston, L. M. Herz and H. J. Snaith, *Energy Environ. Sci.*, 2014, **7**, 982–988.
2 M. A. Green, A. Ho-Baillie and H. J. Snaith, *Nat. Photonics*, 2014, **8**, 506–514.
3 S. D. Stranks, G. E. Eperon, G. Grancini, C. Menelaou, M. J. P. Alcocer, T. Leijtens, L. M. Herz, A. Petrozza and H. J. Snaith, *Science*, 2013, **342**, 341–344.
4 J. H. Heo, S. H. Im, J. H. Noh, T. N. Mandal, C. S. Lim, J. A. Chang, Y. H. Lee, H. J. Kim, A. Sarkar, M. K. Nazeeruddin, M. Gratzel and S. I. Seok, *Nat. Photonics*, 2013, **7**, 487–492.
5 National Center for Photovoltaics at the National Renewable Energy Laboratory, Research cell efficiency records, http://www.nrel.gov/ncpv/, April 2015.
6 G. E. Eperon, V. M. Burlakov, P. Docampo, A. Goriely and H. J. Snaith, *Adv. Funct. Mater.*, 2014, **24**, 151–157.
7 W. Y. Nie, H. H. Tsai, R. Asadpour, J. C. Blancon, A. J. Neukirch, G. Gupta, J. J. Crochet, M. Chhowalla, S. Tretiak, M. A. Alam, H. L. Wang and A. D. Mohite, *Science*, 2015, **347**, 522–525.
8 N. J. Jeon, J. H. Noh, Y. C. Kim, W. S. Yang, S. Ryu and S. I. Seok, *Nat. Mater.*, 2014, **13**, 897–903.
9 J. H. Heo, D. H. Song, H. J. Han, S. Y. Kim, J. H. Kim, D. Kim, H. W. Shin, T. K. Ahn, C. Wolf, T.-W. Lee and S. H. Im, *Adv. Mater.*, 2015, **27**, 3424–3430.
10 Q. Chen, H. P. Zhou, Z. R. Hong, S. Luo, H. S. Duan, H. H. Wang, Y. S. Liu, G. Li and Y. Yang, *J. Am. Chem. Soc.*, 2014, **136**, 622–625.
11 J. Burschka, N. Pellet, S. J. Moon, R. Humphry-Baker, P. Gao, M. K. Nazeeruddin and M. Gratzel, *Nature*, 2013, **499**, 316–319.
12 D. W. deQuilettes, S. M. Vorpahl, S. D. Stranks, H. Nagaoka, G. E. Eperon, M. E. Ziffer, H. J. Snaith and D. S. Ginger, *Science*, 2015, 8.
13 A. Abate, M. Saliba, D. J. Hollman, S. D. Stranks, K. Wojciechowski, R. Avolio, G. Grancini, A. Petrozza and H. J. Snaith, *Nano Lett.*, 2014, **14**, 3247–3254.
14 N. K. Noel, A. Abate, S. D. Stranks, E. S. Parrott, V. M. Burlakov, A. Goriely and H. J. Snaith, *ACS Nano*, 2014, **8**, 9815–9821.
15 J. H. Im, I. H. Jang, N. Pellet, M. Gratzel and N. G. Park, *Nat. Nanotechnol.*, 2014, **9**, 927–932.
16 W. J. Yin, T. T. Shi and Y. F. Yan, *Adv. Mater.*, 2014, **26**, 4653–4658.
17 E. Edri, S. Kirmayer, A. Henning, S. Mukhopadhyay, K. Gartsman, Y. Rosenwaks, G. Hodes and D. Cahen, *Nano Lett.*, 2014, **14**, 1000–1004.
18 H. P. Zhou, Q. Chen, G. Li, S. Luo, T. B. Song, H. S. Duan, Z. R. Hong, J. B. You, Y. S. Liu and Y. Yang, *Science*, 2014, **345**, 542–546.
19 W. J. Yin, T. T. Shi and Y. F. Yan, *Appl. Phys. Lett.*, 2014, 104.

20 S. M. Sze, *Physics of Semiconductor Devices*, John Wiley & Sons, 2nd edn, 1981.
21 F. Deschler, M. Price, S. Pathak, L. E. Klintberg, D. D. Jarausch, R. Higler, S. Huttner, T. Leijtens, S. D. Stranks, H. J. Snaith, M. Atature, R. T. Phillips and R. H. Friend, *J. Phys. Chem. Lett.*, 2014, **5**, 1421–1426.
22 Y. Tian, A. Merdasa, E. Unger, M. Abdellah, K. Zheng, S. McKibbin, A. Mikkelsen, T. Pullerits, A. Yartsev, V. Sundström and I. G. Scheblykin, *J. Phys. Chem. Lett.*, 2015, **6**, 4171–4177.
23 A. Dualeh, N. Tetreault, T. Moehl, P. Gao, M. K. Nazeeruddin and M. Gratzel, *Adv. Funct. Mater.*, 2014, **24**, 3250–3258.
24 V. D'Innocenzo, A. R. S. Kandada, M. De Bastiani, M. Gandini and A. Petrozza, *J. Am. Chem. Soc.*, 2014, **136**, 17730–17733.
25 C. Wehrenfennig, G. E. Eperon, M. B. Johnston, H. J. Snaith and L. M. Herz, *Adv. Mater.*, 2014, **26**, 1584–1589.
26 G. C. Xing, N. Mathews, S. S. Lim, N. Yantara, X. F. Liu, D. Sabba, M. Gratzel, S. Mhaisalkar and T. C. Sum, *Nat. Mater.*, 2014, **13**, 476–480.
27 Y. Yamada, T. Nakamura, M. Endo, A. Wakamiya and Y. Kanemitsu, *J. Am. Chem. Soc.*, 2014, **136**, 11610–11613.
28 S. D. Stranks, V. M. Burlakov, T. Leijtens, J. M. Ball, A. Goriely and H. J. Snaith, *Phys. Rev. Appl.*, 2014, 2.
29 O. D. Miller, E. Yablonovitch and S. R. Kurtz, *IEEE J. Photovoltaics*, 2012, **2**, 303–311.
30 G. E. Eperon, S. N. Habisreutinger, T. Leijtens, B. J. Bruijnaers, J. J. van Franeker, D. W. DeQuilettes, S. Pathak, R. J. Sutton, G. Grancini, D. S. Ginger, R. A. Janssen, A. Petrozza and H. J. Snaith, *ACS Nano*, 2015, **9**, 9380–9393.
31 J. A. Christians, P. A. M. Herrera and P. V. Kamat, *J. Am. Chem. Soc.*, 2015, **137**, 1530–1538.
32 Q. Chen, H. P. Zhou, T. B. Song, S. Luo, Z. R. Hong, H. S. Duan, L. T. Dou, Y. S. Liu and Y. Yang, *Nano Lett.*, 2014, **14**, 4158–4163.

Influence of Growth Temperature on Bulk and Surface Defects in Hybrid Lead Halide Perovskite Films

Citation:

Peng, W., B. Anand, L. Liu, S. Sampat, et al. 2016. "Influence of growth temperature on bulk and surface defects in hybrid lead halide perovskite films." Nanoscale 8(3), doi:10.1039/c5nr06222e.